The hepatitis E virus capsid protein ORF2 counteracts cell-intrinsic antiviral responses to enable persistence in hepatocytes

Ann-Kathrin Mehnert[1,2], Sebastian Stegmaier[2,3#], Carlos Ramirez[4#], Vladimir Gonçalves Magalhães[3], Carla Siebenkotten[1], Jungen Hu[1,2], Ana Luisa Costa[4], Daniel Kirrmaier[5,6], Michael Knop[5,6], Xianfang Wu[7], Thibault Tubiana[8], Carl Herrmann[4], Marco Binder[3], and Viet Loan Dao Thi[1,9*]

[1]Schaller Research Group, Department of Infectious Diseases, Virology, Heidelberg University, Medical Faculty Heidelberg, Heidelberg, Germany; [2]Faculty of Biosciences, Heidelberg University, Heidelberg, Germany; [3]Research Group "Dynamics of Early Viral Infection and the Innate Antiviral Response", Division Virus-Associated Carcinogenesis (D430), German Cancer Research Center (DKFZ), Heidelberg, Germany; [4]Institute for Pharmacy and Molecular Biotechnology, Heidelberg University & BioQuant, Heidelberg, Germany; [5]Center for Molecular Biology of Heidelberg University (ZMBH), Heidelberg, Germany; [6]Division Cell Morphogenesis and Signal Transduction (A260), German Cancer Research Center (DKFZ), Heidelberg, Germany; [7]Infection Biology Program and Department of Cancer Biology, Lerner Research Institute, Cleveland Clinic Foundation, Cleveland, OH, USA; [8]Institute for Integrative Biology of the Cell (I2BC), Université Paris-Saclay, CEA, CNRS, Gif-sur-Yvette, France; [9]German Center for Infection Research (DZIF), Partner Site Heidelberg, Heidelberg, Germany

[#]Authors contributed equally
*Corresponding author: VietLoan.DaoThi@med.uni-heidelberg.de

Classification: Biological Sciences, Microbiology

Keywords: Hepatitis E virus, cell-intrinsic antiviral response, interferon response, viral antagonism, single-cell RNA-sequencing, viral persistence

Electronic word count: 12.328

Number of figures and tables: 5 figures

Abstract

Hepatitis E virus (HEV) is a significant human pathogen causing both acute and chronic infections worldwide. The cell-intrinsic antiviral response serves as the initial defense against viruses and has been shown to be activated upon HEV infection. HEV can replicate in the presence of this response, but the underlying mechanisms remain poorly understood.

Here, we investigated the role of the HEV structural proteins ORF2 and ORF3 in immunocompetent cells. Mechanistically, we validated that ectopic ORF2, but not ORF3, interfered with antiviral and inflammatory signaling downstream of pattern recognition receptors, in part through interaction with the central adaptor protein TANK binding kinase 1. In the full-length viral context, ORF2 contributed to a reduced antiviral response and consequently, more efficient viral replication. In addition, we discovered a protective mechanism mediated by ORF2 that shielded viral replication from antiviral effectors. Using single-cell RNA-sequencing, we confirmed that the presence of ORF2 in infected cells dampened antiviral responses in both actively infected cells and bystanders. As a consequence, we found that early in the infection process, the progression of authentic HEV infection relied on the presence of ORF2, facilitating a balance between viral replication and the antiviral response within immunocompetent cells. Altogether, our findings shed new light on the multifaceted role of ORF2 in the HEV life cycle and improve our understanding of the determinants that may contribute to HEV persistence.

Significance statement

Hepatitis E virus (HEV) is an important yet often underestimated pathogen. Depending on the genotype, HEV infections can progress to chronicity, but the underlying mechanisms remain poorly understood. To gain insight into potential determinants, we investigated how HEV evades the body's first line of defense, the cell-intrinsic antiviral response. We discovered that the HEV capsid protein ORF2 is crucial in limiting this response by interfering with antiviral signaling pathways and shielding viral replication from immune effectors. This balance between viral replication and the antiviral response contributes to persistent HEV infection in immunocompetent cells. Our findings reveal a new role for the HEV capsid protein in the viral life cycle and highlight it as an important target for novel therapeutic approaches.

Introduction

Hepatitis E virus (HEV) is one of the major causes of acute hepatitis across the globe, affecting an estimated 20 million people every year (reviewed in[1,2]). As part of the *Hepeviridae* family, the *Paslahepevirus balayani* genus comprises eight genotypes of which HEV-1 to HEV-4, and more recently HEV-7, have been associated with human infections. HEV-1 and HEV-2 are transmitted fecal-orally and are restricted to humans. In contrast, HEV-3 and HEV-4 spread to humans zoonotically through consumption of meat products from domestic pigs or wild boar. Although HEV-1/-2 infections are usually self-limiting, they are associated with high mortality in pregnant women. Further, HEV-3 and -4 infection of immunocompromised individuals can result in chronicity and development of liver fibrosis and cirrhosis.

HEV is ingested and excreted as a naked virus but circulates in the bloodstream wrapped in a host membrane-derived quasi-envelope, which is acquired during budding from cells (reviewed in[3]). It has a positive-sense, single-stranded RNA genome of approximately 7.2 kilobases, encompassing three open reading frames (ORFs) that give rise to three viral proteins (reviewed in[2]). ORF1 contains the domains involved in viral replication, such as the RNA-dependent RNA polymerase (RdRp). ORF3 is a small phosphoprotein that mediates secretion of viral progeny.

Three distinct isoforms of ORF2 have been described in HEV-infected cells[4-7]. Owing to its N-terminal signal peptide, ORF2 can be secreted along the secretory pathway where it gives rise to the glycosylated (ORF2g) and cleaved (ORF2c) isoforms. ORF2g is secreted as a dimer[5,6] and serves as an immunological decoy *in vivo*[5]. It has been postulated that positively charged residues within an arginine-rich motif (ARM; five arginine residues: RRRGRR) downstream of the signal peptide assist ORF2 in retaining a cytosolic orientation at the endoplasmic reticulum membrane[4]. The intracellular ORF2 isoform (ORF2i) assembles into infectious progenies. ORF2i is mainly located in the cytosol but can translocate to the nucleus, and is likely involved in many virus-host interactions[4,7]. Another study highlighted the importance of two ORF2 start codons. The first start codon can give rise to the secreted ORF2g, while the second gives rise to ORF2i with intracellular localization[5]. Although it remains unclear whether differential usage of these start codons is relevant in HEV infection, they can be used to abrogate expression of individual or all ORF2 isoforms.

Cell-intrinsic defense strategies are initiated by recognition of pathogen-associated molecular patterns (PAMPs) through pattern recognition receptors (PRRs) (reviewed in[8]). In epithelial cells, double-stranded (ds)RNA, the replication intermediate of RNA viruses, is detected by the family of retinoic acid-inducible gene I (RIG-I)-like receptors (RLRs) in the cytosol, including RIG-I and melanoma differentiation-associated protein 5 (MDA5), which are additionally regulated by laboratory of genetics and physiology 2 (LGP2). In the endosome, Toll-like receptor 3 (TLR3) recognizes dsRNA. Different adaptor proteins mediate downstream signaling: Toll/interleukin-1 receptor (TIR) domain-containing adaptor-inducing interferon-β (TRIF) is recruited by TLR3, while RIG-I and MDA5 induce polymerization of mitochondrial antiviral signaling protein (MAVS). Both result in activation of TANK binding kinase 1 (TBK1) and the inhibitor of nuclear factor-κB (IκB) kinase (IKK) complex. TBK1 phosphorylates interferon regulatory factor 3 (IRF3), which translocates into the nucleus and induces expression of type I and type III interferons (IFNs) and IFN-stimulated genes (ISGs). Autocrine and paracrine IFN signaling through Janus kinase/signal transducers and activators of transcription (JAK/STAT) result in expression of hundreds of ISGs

with antiviral functions (reviewed in[9]). Activation of the IKK complex leads to nuclear translocation of nuclear factor-κB (NF-κB) and expression of inflammatory cytokines.

Despite growing interest and advances in recent years, the cell-intrinsic antiviral response to HEV infection remains poorly described. HEV-infected chimpanzees had a similar but weaker ISG response compared to hepatitis C virus (HCV) infection, likely owing to the lower HEV viremia[10]. Infection of innate immunocompetent hepatocyte models with HEV induced robust type III IFN responses, which were dependent on viral replication[11,12]. The induced IFN response appeared to be persistent but was unable to eliminate viral replication within the observed time frames[11,12]. Blunting of IFN induction did not result in enhanced viral replication, suggesting that HEV has developed mechanisms to persistently replicate in the presence of a sustained antiviral response[12]. Corroborating this, several studies have shown that HEV replication is relatively resistant to exogenous IFN treatment, as compared to, for example, HCV[11,13-15]. Yin and colleagues proposed that this is the result of an internal IFN refractoriness due to persistent activation of JAK/STAT1 signaling and retention of phosphorylated STAT1 in the cytosol rather than a direct viral antagonism[11].

Nonetheless, all HEV proteins have previously been suggested to antagonize the cell-intrinsic antiviral response (reviewed in[16]). Within ORF1, the X domain, the putative papain-like cysteine protease (PCP) domain, and the methyltransferase (MeT) domain were shown to interfere with type I IFN induction and NF-κB-mediated signaling[17-20]. A combined MeT-Y-PCP polyprotein was further found to interfere with the JAK/STAT pathway[21]. The ORF2 protein has been reported to interact with TBK1[22,23] and hinder activation of NF-κB[4,24]. Studies of potential ORF3-mediated antagonisms have been controversial: while some studies suggested that ORF3 interferes with type I IFN production, NF-κB-, and IFN-mediated signaling[25-27], one study showed that ORF3 could enhance IFN induction[28]. However, most investigations have relied on overexpression of individual HEV proteins or subdomains of ORF1, and the physiological relevance of each antagonism for HEV replication remains elusive.

In the present study, we sought to clarify the role of HEV ORF2 and ORF3 proteins in antagonizing antiviral responses and their contribution to the progression of HEV infection. To address this, we made use of viral mutants and assessed differences in IFN and ISG responses upon authentic infection of different immunocompetent hepatocellular systems in bulk and at single-cell resolution. We identified a replication-limiting bottleneck mediated by the antiviral response early in infection that is overcome by the capsid protein ORF2, but not ORF3, allowing for the establishment of persistent viral replication.

Results

The HEV ORF2 protein antagonizes both antiviral and inflammatory signaling pathways and interacts with TBK1

Several independent studies have reported that HEV ORF2 and ORF3 antagonize different steps of the cell-intrinsic antiviral response, however, with a variety of different conclusions[22-27]. Therefore, we aimed to mechanistically dissect at which steps ORF2 and ORF3 interfere with antiviral and inflammatory signaling. Importantly, we clearly separated our analysis between IFN induction and IFN signaling as well as systematically compared the roles of ORF2 and ORF3 side by side.

144 We first focused on sensing and signaling by PRRs. For this mechanistic investigation, we
145 made use of readily available A549-derived cell lines, which harbor a double knockout of RIG-I
146 and MDA5 and show negligible TLR3 expression[29]. In addition to reconstitution with weak
147 transgene overexpression of either MDA5[30], RIG-I[30], or TLR3, we ectopically expressed HEV
148 ORF2, ORF3, or GFP in these cells. In GFP-expressing cells, stimulation of the respective PRR
149 with Mengo-Zn virus, Sendai virus (SeV), and poly(I:C) supernatant feeding resulted in the
150 induction of *IFNB1* expression (Fig. 1A-C). Ectopic expression of HEV ORF3 did not significantly
151 alter *IFNB1* expression downstream of RIG-I and MDA5 (Fig. 1A-B) but resulted in a minor
152 enhancement downstream of TLR3 compared to the GFP control (Fig. 1C). In cells expressing
153 ectopic ORF2, *IFNB1* induction was significantly lower downstream of all PRRs compared to
154 GFP-expressing cells (Fig. 1A-C). Not only ORF2 from a chronic HEV genotype (HEV-3) but also
155 from an acute genotype (HEV-1) dampened this response (Fig. 1A-C). By ELISA, we confirmed
156 that ectopic ORF2 expression also decreased IFNβ protein secretion (Suppl. fig. 1A-C). While the
157 presence of ectopic ORF2 dampened the strength of *IFNB1* induction, it did not alter the dynamics
158 of RLR signaling, which we tested by time-resolved RT-qPCR analysis of MDA5-expressing cells
159 electroporated with poly(I:C) (Suppl. fig. 1D-E).
160 We further investigated the impact of ORF2 expression on inflammatory and cytokine-
161 dependent antiviral signaling. Upon TNF stimulation, the presence of ectopic ORF2, but not
162 ORF3, reduced the induction of the inflammatory cytokine *TNFAIP3* significantly (Fig. 1D), thus
163 interfering with NF-κB-dependent signaling. On the other hand, we did not observe significant
164 differences in expression of the ISG *IFIT1* upon stimulation with IFNβ in the presence of either
165 ectopic ORF2 or ORF3, suggesting that neither interfered with JAK/STAT signaling (Fig. 1E).
166 Our results demonstrated that ORF2 interferes with the sensing pathway upstream of IFN
167 induction and with NF-κB-dependent inflammatory cytokine induction downstream of the TNF
168 receptor, similar to previous literature[22-24]. ORF3 did not affect antiviral and inflammatory
169 responses as strongly as proposed previously[25-28]. Importantly, IFN-mediated signaling was not
170 affected by either of the viral proteins. As NF-κB-dependent cytokine induction is particularly
171 important for the crosstalk with immune cells *in vivo*, we continued focusing on the effects of
172 ORF2 on the antiviral IFN/ISG response.
173 It was previously suggested that ORF2 interacts with the critical adaptor molecule TBK1,
174 likely through the ARM[23], but a direct interaction through this motif was not analyzed. Here, we
175 confirmed the interaction of HEV-3 ORF2 and TBK1 by co-immunoprecipitation (co-IP) (Fig. 1F).
176 We further found that mutation of the last two arginine residues of the ARM to alanine (2R/2A)
177 decreased the interaction of TBK1 with ORF2 (Fig. 1F). However, this particular mutation
178 abrogates nuclear translocation of ORF2i and increases ORF2 secretion and glycosylation along
179 the secretory pathway[4]. Hence, the pool of cytosolic ORF2i is reduced[4] and thus, also the
180 likelihood of interaction with TBK1. In agreement with this, the ORF2-2R/2A protein appeared with
181 a light smear in our Western blot (WB) analysis as compared to WT ORF2, suggesting the
182 presence of post-translational modifications such as glycosylation (Fig. 1F).
183 In an effort to determine other potential interaction motifs between ORF2 and TBK1, we
184 made use of AlphaFold. Repeated modeling identified the last three residues of the LGSA<u>WRD</u>
185 motif (spanning amino acids 83 to 89) at the N-terminus of ORF2 as the only promising, putative
186 interaction motif (Suppl. fig. 2A, 2C-E). However, mutation of these residues to triple alanine did

187 not result in impaired interaction between ORF2 and TBK1, suggesting that this predicted motif
188 is not essential (Suppl. fig. 2B).
189 Altogether, we systematically validated in a side-by-side comparison that ORF2 but not
190 ORF3 counteracts IFN induction downstream of all relevant PRRs and additionally interferes with
191 NF-κB-mediated signaling. The antagonism of the antiviral response by ORF2 is mediated at least
192 in part by interaction with TBK1, although the precise interaction motif remains elusive.
193
194 *The capsid protein ORF2, but not the ORF3 protein, is pivotal for efficient HEV replication in*
195 *immunocompetent cells*
196 HEV replication in hepatocytes persists in the presence of a sustained cell-intrinsic
197 antiviral response[11,12]. To study how far HEV replication is dependent on ORF2-mediated escape
198 of the antiviral response, we generated a ΔORF2 and a control ΔORF3 mutant of the HEV-3
199 Kernow-C1/p6 (wild type, WT) strain (Fig. 2A). To obtain ΔORF2, we mutated the two start codons
200 of *ORF2* to abrogate protein expression of all ORF2 isoforms without affecting correct translation
201 of the overlapping *ORF3*, as suggested by Yin *et al.*[5]. Upon electroporation (EPO) into
202 immunocompetent HepG2/C3A cells[11,31], we observed significantly reduced replication of the
203 ΔORF2 mutant compared to both WT and the ΔORF3 mutant on day 5 and day 7 post-EPO (Fig.
204 2B). Of note, at least part of the basal HEV RNA detected up to day 3 post-EPO resulted from
205 high levels of incoming, electroporated RNA, as revealed by comparison with a replication-
206 incompetent GNN mutant of the RdRp (Fig. 2B). *IFNL1* (Fig. 2C) and *ISG15* induction (Fig. 2D)
207 upon HEV WT, ΔORF3, but also ΔORF2 replication was similar on day 1 and day 3 post-EPO.
208 However, we observed significantly stronger expression of both antiviral response genes for
209 ΔORF2 on day 5 post-EPO (Fig. 2C-D), coinciding with the decrease in ΔORF2 viral RNA (Fig.
210 2B). While induction of *IFNL1* and *ISG15* was not significantly different from WT and ΔORF3 on
211 day 7 post-EPO, the 8.6-fold lower levels of ΔORF2 RNA compared to WT RNA (Fig. 2B)
212 indicated a relatively stronger antiviral response induction for ΔORF2 (Fig. 2C-D and Suppl. fig.
213 3A-B).
214 Importantly, we did not observe induction of *IFNL1* (not detectable) or *ISG15* expression
215 (Fig. 2D) upon EPO with the replication-incompetent GNN mutant. We therefore concluded that
216 the incoming RNA and consequently, the full-length single-stranded HEV genome was not sensed
217 by PRRs. Hence, we excluded the possibility that the differences in the antiviral response we
218 observed for ΔORF2 were the results of increased sensing of unpackaged HEV genome due to
219 the missing capsid protein ORF2. Furthermore, we ruled out effects of ORF2 and ORF3 deletion
220 on secondary virus spread because ΔORF3 replicated at WT levels and ORF3 is the protein
221 responsible for secretion of progeny. In addition, newly produced virus particles released into the
222 supernatant are quasi-enveloped and therefore, not highly infectious[32].
223 We hypothesized that the antiviral response induced in the absence of ORF2 was strong
224 enough to cause, at least in part, the observed decline in viral replication. In order to address this,
225 we exogenously inhibited IFN and ISG induction by treating the cells with the drug BX795, which
226 inhibits the target of the ORF2 antagonism, TBK1. Prolonged incubation with BX795 can affect
227 cell viability, as TBK1 is also involved in many other cellular processes. To minimize such effects
228 (Suppl. fig. 3C-E), we incubated the cells with BX795 for only 48 h before harvesting. Application
229 of BX795 reduced *IFNL1* and *ISG15* induction in response to viral replication (Suppl. fig. 3F-H).
230 HEV WT replication was not significantly enhanced (Fig. 2E), while ΔORF3 replication showed

231 only a minor increase (Fig. 2G). In contrast, the BX795 treatment resulted in a significant and
232 stronger increase in ΔORF2 replication, especially on day 5 and day 7 post-EPO (Fig. 2F). This
233 implied that the antiviral response had a greater effect on viral replication in the absence of ORF2.
234 To study this observation at the single-cell level, we detected HEV genomes by RNA-
235 fluorescence *in situ* hybridization (RNA-FISH) (Fig. 2H), allowing us to quantify the percentage of
236 HEV-infected cells over time, independent of viral antigen expression. As early as day 3 post-
237 EPO, ΔORF2 RNA signals were weaker compared to WT and ΔORF3 and continued to decline
238 thereafter (Fig. 2H-I). Analogous to our results in Fig. 2B, the decrease in WT- and ΔORF3-
239 positive cells from day 3 to day 5 post-EPO was likely due to the detection of residual incoming
240 RNA on day 3, introduced by the EPO process (Fig. 2I). Overall, the percentages of WT- and
241 ΔORF3-positive cells remained comparable between day 5 and day 7 post-EPO (Fig. 2I). In
242 contrast, we barely detected ΔORF2 RNA at these days as evidenced by a significant decrease
243 compared to day 3. Interestingly, ΔORF2 RNA was still detectable in our bulk RT-qPCR analysis
244 at these time points (Fig. 2B). Importantly, the RNA-FISH assay is based on the hybridization of
245 20 probe pairs to an *ORF2* target region spanning approximately 1,000 nucleotides[33], whereas
246 RT-qPCR only amplifies a short sequence stretch of 70 nucleotides. Therefore, it is possible that
247 we detected many degraded ΔORF2 genomes by RT-qPCR at day 5 and day 7 post-EPO.
248 Next, we aimed to determine whether the absence of ORF2 resulted in increased
249 sensitivity of viral replication to the action of antiviral effectors. To focus solely on the effects of
250 ISGs, we used Huh7.5 cells, which are only weakly responsive to PRR stimulation due to a non-
251 functional RIG-I and negligible basal expression of MDA5[34], TLR3[34], and LGP2[35]. Therefore, HEV
252 replication should not induce an antiviral response. Indeed, EPO of Huh7.5 cells with WT and
253 ΔORF2 RNA resulted in comparable viral replication (Suppl. fig. 4A), likely due to the lack of an
254 antiviral response in these cells (Suppl. fig. 4B). Next, we treated WT- and ΔORF2-electroporated
255 Huh7.5 cells four days post-EPO with either IFNλ1 or IFNα2A for 72 h to induce ISG expression.
256 Comparable ISG induction between WT and ΔORF2 further confirmed that ORF2 did not interfere
257 with JAK/STAT signaling (Suppl. fig. 4C-D). Importantly, we detected neither *IFNB1* nor *IFNL1*
258 expression upon IFN treatment of WT- and ΔORF2-electroporated cells. Thus, we could exclude
259 the possibility that the IFN treatment led to an upregulation of PRR expression and consequently,
260 an increased ISG induction in a positive feedback loop due to enhanced sensing of HEV RNA.
261 Nonetheless, we observed that ΔORF2 replication was more strongly inhibited by IFN treatment
262 and the ensuing ISG response than WT replication (Fig. 2J). We therefore concluded that ΔORF2
263 replication was more sensitive to the antiviral effects of ISGs induced by exogenous IFN
264 treatment, even in the absence of a directly virus-induced antiviral response. We therefore
265 concluded that this additional protective role of ORF2 further contributed to the decrease in viral
266 replication in the absence of ORF2 (Fig. 2B).
267 Altogether, we found that the presence of ORF2 is critical for efficient HEV replication due
268 to a dampened cell-intrinsic antiviral response. Further, the absence of ORF2 resulted in
269 increased sensitivity of HEV replication to the action of ISGs, suggesting additional protective
270 functions of the ORF2 protein, independently of its direct interaction with TBK1.
271
272
273

274 *A balance between HEV replication and the antiviral response at an early infection bottleneck is*
275 *essential for sustained viral replication*
276 We next sought to identify the time point at which the presence of ORF2 is decisive for
277 the fate of HEV replication in authentic infection. To this end, we established a trans-
278 complementation system in hepatoma S10-3 cells ectopically expressing ORF2 to produce
279 ΔORF2 virus particles (Fig 3A), similar to trans-complementation of a subgenomic replicon
280 described previously[36]. Ectopic ORF2 expression was comparable to the protein level reached by
281 viral replication after EPO of WT HEV RNA into naïve S10-3 cells (Fig. 3B). We further confirmed
282 by WB that ORF3 but not ORF2 was expressed upon EPO of ΔORF2 RNA into naïve cells (Fig.
283 3B). We then harvested infectious ΔORF2 particles from ORF2-expressing S10-3 cell lysates to
284 perform HEV infections.
285 Next, we aimed to study the replication dynamics after cell entry in HepG2/C3A cells in a
286 time-resolved manner. We synchronized the infection at equal MOI (30 genome equivalents
287 (GE)/cell) of both WT and ORF2-trans-complemented HEV particles by a binding step for 2 hours
288 (h) at 4 °C and internalization for 8 h at 37 °C after which the inoculum was removed, referred to
289 as day 0 post-internalization. We analyzed viral replication and the antiviral response every 8 h
290 between day 1 and day 3 post-internalization and every day (i.e., every 24 h) thereafter by RT-
291 qPCR. Despite infection with the same number of GEs, ΔORF2 HEV RNA levels detected after
292 internalization were always approximately 2.4-fold lower than WT HEV RNA (Suppl. fig. 5A). This
293 indicated a lower specific infectivity of the trans-complemented ΔORF2 virus particles, potentially
294 due to less efficient progeny assembly. For easier comparison, we therefore normalized HEV
295 RNA over day 0 post-internalization.
296 Replication of WT and the ΔORF2 mutant peaked at 48±8 h post-internalization, followed
297 by a decline (Fig. 3C). Interestingly, while the HEV WT replication leveled off between 56 h and
298 day 7 post-internalization (2.0-fold decrease), ΔORF2 replication continued to decrease
299 significantly by 8.5-fold between those two time points. Following the onset of viral replication, we
300 observed an increase in *IFNL1* (Fig. 3D) and *ISG15* expression (Fig. 3E), which peaked at 56 h
301 and 64 h, respectively. Following the decrease in viral replication, *IFNL1* and *ISG15* levels also
302 declined. *IFNL1* and *ISG15* expression for ΔORF2 was not significantly different from WT at 56 h
303 and on day 7 post-internalization (Fig. 2D-E). However, considering the fact that ΔORF2 RNA
304 significantly decreased until day 7 compared to WT RNA (Fig. 2C), the comparable *IFNL1* and
305 *ISG15* induction between WT and ΔORF2 suggested a relatively stronger antiviral response in
306 ΔORF2 infection (Suppl. fig. 5B-C). Importantly, we did not detect an antiviral response following
307 HEV internalization (day 0) (Fig. 3D-E). This is in agreement with our earlier finding that the
308 incoming RNA and thus, the full-length single-stranded HEV RNA is not being sensed by the cells.
309 Next, we aimed to validate our findings in a more physiologically relevant hepatocellular
310 system. To this end, we used human pluripotent stem cell-derived hepatocyte-like cells (HLCs)
311 which are permissive to HEV infection[12,32] (Fig. 3F). We infected HLCs overnight at equal MOI
312 (30 GE/cell) with HEV WT and ΔORF2 virus particles produced by trans-complementation. Similar
313 to our results in infected HepG2/C3A cells, ΔORF2 RNA was lower than WT on day 1 post-
314 infection, likely due to a lower specific infectivity as discussed above. Nonetheless, we observed
315 decreased ΔORF2 replication over time (Fig. 3G), accompanied by a significantly stronger
316 induction of *ISG15* compared to HEV WT on day 5 and day 7 post-infection (Fig. 3H).

317 Overall, our observations suggest that the presence of the ORF2 protein is critical for
318 establishing an equilibrium between viral replication and the antiviral response early in infection,
319 allowing HEV to replicate in different immunocompetent hepatocellular systems.
320
321 *scRNA-seq analysis reveals globally dampened and partly divergent ISG responses in HEV-*
322 *infected cells and bystanders in the presence of ORF2*
323 Expression of ISGs can be induced immediately downstream of viral recognition by PRRs
324 (reviewed in[9]). In addition, secreted IFN can lead to amplified ISG induction in an auto- and
325 paracrine manner. In HEV infection, it remains unclear whether IFN and ISG responses observed
326 in bulk analyses such as RT-qPCR are derived from infected cells, uninfected bystanders, or
327 possibly both. ISG responses from uninfected bystanders only could be induced by low levels of
328 IFN secretion from infected cells. Alternatively, viral RNA transfer to neighboring cells via
329 extracellular vesicles could lead to IFN and ISG induction in bystanders, similar to what has been
330 described for HCV and other viruses (reviewed in[37]).
331 To identify the cellular origin of the antiviral response in HEV infection and assess potential
332 differences in the response in the absence of ORF2, we performed single-cell RNA-sequencing
333 (scRNA-seq) using microfluidics-based 3'-targeted 10x Genomics. To this end, we infected
334 HepG2/C3A cells with HEV WT and trans-complemented ΔORF2 virus particles in a synchronized
335 manner as described above and analyzed the cells at 56 h post-internalization. This time point
336 represents the antiviral response-mediated bottleneck we identified to be essential for persistent
337 replication in the presence of ORF2 (Fig. 3C-E). Since the ΔORF2 virus replicates to almost
338 undetectable levels at later time points, we only analyzed HEV WT-infected cells on day 7 post-
339 infection.
340 We first performed a gene set enrichment analysis of the HEV WT- and ΔORF2-infected
341 samples compared to the uninfected sample at 56 h, using the hallmark gene sets of the Human
342 MSigDB Collections[38]. Interferon alpha and gamma responses were among the most significantly
343 upregulated gene sets, in both HEV WT and ΔORF2 infection, highlighting that the global
344 response was dominated by differential expression of ISGs (Fig. 4A-B). Enrichment of oxidative
345 phosphorylation and glycolysis gene sets indicated increased metabolic activity of the infected
346 samples. Analysis of HEV WT infection on day 7 showed that the enriched gene sets were
347 comparable over time and interferon-related responses were still prominently enriched (Fig. 4C).
348 Next, we clustered the uninfected, HEV WT-, and ΔORF2-infected samples at 56 h based
349 on a list of approximately 400 ISGs published previously by Schoggins *et al.*[39] (Fig. 4D-G). This
350 revealed two major subpopulations in the infected samples (Fig. 4E-F), also on day 7 (Suppl. fig.
351 6A-C). We concluded that the cells located in the cluster overlapping with the uninfected sample
352 were non-responding cells, characterized by unchanged ISG expression. The cells located in the
353 second cluster showed differential ISG expression compared to the non-responding cells and
354 were thus classified as responders, from here on called the active cluster (Fig. 4H). In agreement
355 with the globally enhanced metabolic activity (Fig. 4A-B), this cluster appeared to be more
356 transcriptionally active, as indicated by an increased number of expressed genes (Fig. 4I) as well
357 as an overall increased number of transcripts (Suppl. fig. 6E). Within the WT- and ΔORF2-infected
358 samples, 28.1% and 17.2% of cells were identified as HEV RNA-positive, respectively (Suppl. fig.
359 6F). Interestingly, we observed that most infected cells of both WT- (Fig. 4J) and ΔORF2-infected
360 samples (Fig. 4K) were located in the active cluster, together with uninfected bystanders. We

361 therefore concluded that both actively infected cells and uninfected bystanders responded by
362 upregulated ISG expression. Although detectable by qRT-PCR (Fig. 3D), we could not detect type
363 III IFN gene expression in the infected samples via scRNA-seq, likely due to low numbers of IFN
364 transcripts per cell. Therefore, we could not identify whether only infected cells or also uninfected
365 bystanders were the source of IFN. Nonetheless, we could demonstrate that the ISG response
366 was not fully suppressed in actively infected cells by the ORF2 antagonism.
367 Compared with the infected cells in the active cluster, the few infected cells located within
368 the inactive cluster had lower HEV RNA counts (Suppl. fig. 6G). These cells might be at an earlier
369 stage of infection due to a delayed onset of replication or due to secondary infection, which,
370 however, should be limited at this early time point. Finally, not only uninfected bystanders but also
371 HEV-infected cells still showed enhanced ISG expression and localized to the active cluster on
372 day 7 post-HEV WT infection (Suppl. fig. 6D). This provided further evidence that the
373 establishment of an equilibrium between HEV replication and the antiviral response early in
374 infection is essential for persistent viral replication in an antiviral environment.
375 Next, we sought to examine the specific ISG signatures (i.e., the set of ISGs) induced
376 upon WT and ΔORF2 infection. We compared the respective lists of differentially expressed ISGs
377 in the active clusters of WT and ΔORF2 infection and found that out of 243 differentially expressed
378 ISGs, 79.8% overlapped (Fig. 4J and Suppl. table 2). This was further substantiated by
379 identification of ISGs specifically upregulated in actively infected cells, defined by detection of at
380 least one HEV RNA copy per cell, or bystanders, defined by the absence of HEV RNA, in the
381 active clusters of WT- (Suppl. fig. 7A) and ΔORF2-infected samples (Suppl. fig. 7B). Actively
382 ΔORF2-infected cells expressed a larger subset of differing ISGs compared to WT-infected cells
383 (Suppl. fig. 7A). We therefore concluded that the ISG signatures induced by WT and ΔORF2
384 infection are not entirely identical.
385 Next, we compared the strength of ISG induction in actively infected cells and uninfected
386 bystanders within the active cluster. We observed a globally stronger ISG response in ΔORF2-
387 infected cells and bystanders compared to WT infection (Fig 4I), indicating overall increased IFN
388 production and secretion, despite remaining undetectable by scRNA-seq. Consulting the list of
389 overlapping, significantly upregulated ISGs identified in Fig. 4L (and Suppl. table 2) and previous
390 literature on the upregulation of ISGs in HEV infection of different hepatocellular systems and in
391 chimpanzees[10-12,40], we selected a subset of ISGs for further comparison of infected cells and
392 bystanders. These common differentially expressed genes further substantiated a globally
393 stronger ISG response in both infected cells and uninfected bystanders in the active cluster of the
394 ΔORF2-infected sample compared with the respective cell populations of the WT-infected sample
395 (Fig. 4N).
396 Overall, we identified both actively infected cells and uninfected bystanders to be the
397 cellular origins of ISG responses at early and later time points of HEV infection. Early in infection,
398 the absence of ORF2 results in induction of a globally stronger and partially divergent ISG
399 signature in infected cells. In addition, increased autocrine and paracrine IFN signaling, when not
400 dampened by the presence of ORF2, leads to enhanced ISG responses in both infected cells and
401 bystanders.
402
403
404

405 **Discussion**

406 HEV replication has been shown to persist despite a sustained cell-intrinsic antiviral
407 response. However, an in-depth understanding of the underlying mechanisms and the active
408 contribution of a viral antagonism is missing. In this study, we analyzed authentic HEV infection
409 with mutants lacking expression of individual viral proteins at single-cell resolution. We identified
410 a replication-limiting bottleneck imposed by the antiviral response where the presence of ORF2
411 and thus, likely its interaction with the adaptor molecule TBK1 determine whether viral replication
412 declines or equilibrates with the antiviral response (summarized in Fig. 5).
413
414 *Single-cell analysis uncovers the role of the multifunctional capsid protein for HEV persistence*
415 *amidst an antiviral environment*

416 In the present study, we have shown that the capsid protein ORF2 is a critical viral
417 determinant of HEV replication efficiency. In absence of the ORF2 protein, a stronger cell-intrinsic
418 antiviral response is induced. Importantly, we ruled out that the full-length, single-stranded HEV
419 genome was sensed because the replication-incompetent GNN mutant did not induce IFN or ISG
420 expression (Fig. 2C-D). Otherwise, sensing of accumulating unpackaged HEV genome due to the
421 missing capsid protein ORF2 could have explained the enhanced antiviral response. A previous
422 study has suggested that the 3'-untranslated region (UTR) of single-stranded HEV RNA is sensed
423 by RIG-I[41]. However, as the authors used transfection of short RNA fragments, which are ideal
424 PAMPs for RIG-I, we hypothesize that this might be rather irrelevant in authentic HEV infection
425 and that double-stranded replication intermediates might be sensed instead.

426 Investigation of the cell-intrinsic antiviral response at the single-cell level revealed that
427 both infected cells and uninfected bystanders are the source of the ISG response in HEV infection.
428 The ISG response in both cell types was globally stronger in the absence of ORF2 (Fig. 4M-N).
429 Thus, the ORF2-mediated viral antagonism does not completely suppress antiviral responses
430 within infected cells. Instead, it reduces ISG and presumably IFN induction within infected cells
431 and consequently further ISG induction via autocrine and paracrine IFN signaling. Absence of
432 ORF2 further allows expression of a partially divergent ISG subset. It remains to be clarified
433 whether these ISGs might be particularly potent in restricting viral replication. Overall, ORF2
434 contributes to dampening of the antiviral responses below a critical threshold, allowing viral
435 replication and the antiviral response to reach an equilibrium where they can coexist. We propose
436 that this equilibrium is a prerequisite for persistent HEV infection. Future studies are needed to
437 determine whether IFN is produced only by infected cells or also by uninfected bystanders, and
438 to characterize the role of secreted ORF2 isoforms in influencing paracrine immune signaling.

439 HEV ORF2 appears to be a multifaceted protein with a wide range of functions affecting
440 different host pathways. In addition to its direct involvement in immune evasion downstream of
441 PRR recognition, we speculate that the capsid protein ORF2 may also exert additional, protective
442 functions. Here, we demonstrated that ORF2 is essential for maintaining the relative resistance
443 of HEV to type I and type III IFN treatment, even in the absence of a virus-induced antiviral
444 response (Fig. 2J). Importantly, we were able to exclude a direct inhibition of IFN signaling by
445 ORF2 (Fig. 1E). Therefore, we concluded that the capsid protein additionally contributes to the
446 shielding of replicating RNA from the action of ISGs and potentially also from recognition of
447 double-stranded replication intermediates by PRRs.

448 Most positive-sense RNA viruses replicate in the cytosol and restructure their host cell by
449 inducing host membrane-derived replication compartments (reviewed in[42]). While such replication
450 organelles have not yet been reported for HEV, several studies have suggested that different
451 compartments of the endolysosomal system or the ER-Golgi intermediate compartment (ERGIC)
452 could be involved[43-46]. ORF2 was frequently detected at these proposed replication sites.
453 Therefore, it may be involved in either remodeling or redirecting cellular structures to help create
454 the replication site, thereby potentially contributing to protection of viral RNA from the antiviral
455 effects of induced ISGs.
456 Despite the relatively low abundance of ORF1 and ORF3 proteins compared to ORF2
457 protein in authentic infection[47], we cannot exclude the possibility that these proteins have
458 additional potential to interfere with antiviral signaling and contribute to viral persistence.
459 Ectopically expressed ORF3 may interact with components of the antiviral response as reported
460 by others[25-27]. In this study however, we did not observe any striking effects of ORF3 on viral
461 replication and antiviral responses. Furthermore, the processing of the ORF1 polyprotein in
462 authentic infection remains controversial (reviewed in[48]). Therefore, physiologically relevant
463 contributions of the previously reported antagonisms by ORF1 to the overall persistence
464 phenotype remain to be confirmed.
465
466 *The direct interaction of HEV ORF2 with TBK1 is critical for antagonizing replication-limiting*
467 *responses*
468 There is no convincing evidence for a viral protease encoded by the HEV genome. Indeed,
469 unlike HCV[49] or HAV[50], HEV does not cleave MAVS[11], a key adaptor molecule in the induction of
470 cell-intrinsic antiviral responses. Instead, HEV appears to have developed other counteractive
471 strategies. In agreement with previous literature[22,23], we found that the HEV ORF2 protein
472 interacts directly with TBK1 to dampen IFN induction. This could be directly involved in impairing
473 the establishment of an infection-limiting antiviral state. Here, we identified an early time point at
474 which the presence of ORF2 is critical for the progression of authentic HEV infection, facilitating
475 a balance between viral replication and the antiviral response within immunocompetent cells.
476 Lin and colleagues[23] previously suggested that the ARM of ORF2 is responsible for the
477 inhibition of TBK1-induced phosphorylation of IRF3. Indeed, we could show a reduced interaction
478 between ORF2 and TBK1 upon mutation of the ARM. However, this motif has also been identified
479 as the master regulator of the ORF2 isoforms[4]. Therefore, mutating the ARM could also indirectly
480 affect interference with the antiviral response, as enhanced secretion of glycosylated ORF2 along
481 the secretory pathway results in decreased cytosolic and nuclear availability of ORF2 to interact
482 with TBK1 and other unidentified factors. Furthermore, we found that ORF2 also antagonizes NF-
483 κB-dependent cytokine induction (Fig. 1D) and is hence likely to interfere with additional
484 components other than TBK1. This observation is in agreement with the previously published
485 interaction of ORF2 with beta-transducin repeat containing protein (βTRCP)[24], which resulted in
486 reduced proteasomal degradation of the inhibitory complex of NF-κB. Additionally, nuclear
487 translocation of ORF2 has been proposed to affect inflammatory cytokine induction[4]. Considering
488 the numerous suggested ORF2 antagonisms by us and others, we believe that viral persistence
489 is likely based on combinatorial interference of ORF2 with different pathways.
490 Due to the apparent multifunctionality of the ORF2 protein, individual functions are difficult
491 to untangle if specialized domains remain unknown. Indeed, our attempts to predict any putative

492 interaction sites between ORF2 and TBK1 with AlphaFold remained unsuccessful. The only
493 promising prediction was localized to the N-terminus of ORF2, however, this portion of the ORF2
494 protein appears to be intrinsically disordered[51]. While AlphaFold has demonstrated success in
495 identifying binding regions between other viral proteins and host factors[52], this particular
496 interaction highlights the challenges of accurately predicting interactions involving disordered
497 protein regions[53,54]. This complexity could stem from several factors: AlphaFold heavily relies on
498 co-evolutionary signals, which might be less pronounced in this virus-host interaction. Instead,
499 the ORF2-TBK1 interaction may rather be driven by physico-chemical properties that are not
500 explicitly considered in AlphaFold's predictions. Finally, the N-terminus of ORF2 may adopt a
501 specific structure upon interaction with TBK1, as is the case for many intrinsically disordered
502 proteins (reviewed in[55]). High-resolution structural studies of TBK1-ORF2 complexes may
503 therefore be required to further identify the interacting regions.
504
505 *Innate immunity as a potential determinant of HEV chronicity and species tropism*
506 Infections with different HEV genotypes result in distinct clinical outcomes. While HEV-1
507 infections are acute and self-limiting, HEV-3 infections can become chronic in
508 immunocompromised individuals. The determinants of these intergenotypic differences remain to
509 be elucidated, but innate and adaptive immune responses are likely critical parameters (reviewed
510 in[16]).
511 We have previously shown that infection with an HEV-1 isolate resulted in a stronger IFN
512 and ISG response than infection with an HEV-3 isolate. Interestingly, HEV-1 but not HEV-3
513 replication appeared to decrease thereafter[12]. Why HEV-1 induces a stronger response and
514 whether this contributes to the self-limiting course of infection observed in humans and in HEV-
515 1-infected chimpanzees[10] should be investigated in the future.
516 On the other hand, a moderate but prolonged cell-intrinsic IFN response induced by HEV-
517 3 could help to induce tolerance and dampen the effect of the stronger type I IFN response elicited
518 by professional immune cells such as plasmacytoid dendritic cells (pDCs). In agreement, we and
519 others have demonstrated a remarkable resistance of HEV replication to exogenous IFN once
520 replication is fully established[11,13-15]. Continuous activation of JAK/STAT signaling upon HEV
521 replication has been shown to render the cells refractory to exogenous IFN stimulation[11]. A recent
522 publication further suggested that ORF2 isoforms modulate detection of HEV-infected cells by
523 pDCs, indicating that this cell type might be contributing to HEV control *in vivo*[31]. Not only do pDCs
524 produce IFN and other cytokines to activate innate immune cells, but they also capture and
525 process antigens to initiate adaptive T cell responses. Consequently, a reduced T cell activation
526 could be beneficial for establishing HEV persistence *in vivo*. Studying the crosstalk with immune
527 cells will be pivotal for identifying determinants of chronicity.
528 Our results showed no difference in the potential of ORF2 from acute and chronic
529 genotypes to interfere with IRF3- and NF-κB-mediated signaling (Figure 1), which is consistent
530 with previous studies[22,23]. However, this could play a role in the genotype-dependent species
531 tropism of HEV. While HEV-1 is limited to primates and human infection, HEV-3 can infect a wide
532 range of animals and is mainly transmitted zoonotically to humans. Interaction of ORF2 with TBK1
533 could potentially represent a prime example of the ongoing arms race between virus and host,
534 driving the co-evolution of viral evasion strategies and host defenses. Therefore, future research
535 should investigate the differences in the ability of HEV-1 and HEV-3 ORF2 to counteract TBK1

536 from different HEV-3 host species, including pig or rabbit. Such studies might contribute to the
537 identification of the determinants of HEV species tropism.
538 Many open questions remain about the mechanisms of HEV persistence. In this study, we
539 have shown that the HEV capsid protein ORF2 mediates a viral antagonism affecting both antiviral
540 and inflammatory signaling. ORF2 is essential at a replication-limiting bottleneck early in infection
541 mediated by the antiviral response, which is decisive for establishment of persistent viral
542 replication. We have also laid the groundwork for future studies to focus on the role of
543 intergenotypic differences in the antiviral response and crosstalk with immune cells. This could
544 eventually lead to a better understanding of the determinants of acute and chronic manifestations
545 of HEV infection, which will be valuable in identifying novel therapeutic regimens.
546
547 **Materials and Methods**
548 *Standard cell culture*
549 The human hepatoma cell lines HepG2/C3A (ATCC HB-8065), Huh7.5 (a kind gift from
550 Charles Rice, The Rockefeller University), S10-3 (a kind gift from Suzanne Emerson, NIH), and
551 derived S10-3/ORF2 as well as the human embryonic kidney cell line HEK293T (ATCC CRL-
552 3216) were cultured in Dulbecco's Modified Eagle Medium (DMEM, Gibco, high glucose,
553 GlutaMAX supplement) with 10% fetal bovine serum (FBS, Capricorn) and 1%
554 penicillin/streptomycin (pen/strep), referred to as complete DMEM (cDMEM). HepG2/C3A cells
555 were grown on collagen-coated cell culture vessels. A549-derived cell lines were cultured in
556 DMEM (Gibco, high glucose) with 10% FBS (Pan Biotech), 1% pen/strep, and 1% non-essential
557 amino acids (NEAA). Cell lines with ectopic protein expression were produced by standard
558 lentiviral transduction, selected, and continuously cultured under respective antibiotic selection
559 pressure. Cells were maintained at 37 °C in 95% humidity and 5% CO_2 atmosphere. All cell lines
560 used in this study routinely tested negative for mycoplasma.
561
562 *Stimulation of PRR-overexpressing A549-derived cell lines*
563 $1x10^5$ A549-derived cell lines were seeded in 24-well plates. The next day, cells were
564 infected with Mengo-Zn virus[56] (MOI 1) for 24 h, Sendai virus (SeV, MOI 0.75; prepared from
565 allantoic fluid of embryonated chicken eggs, a kind gift from Rainer Zawatzky, German Cancer
566 Research Center (DKFZ), Heidelberg, Germany) for 4 h, or supernatant-fed with high molecular
567 weight (HMW) poly(I:C) (InvivoGen) at 50 µg/mL for 24 h in DMEM containing 2% FBS, 1% NEAA,
568 and 1% pen/strep. Stimulation with TNF (Abcam) at 10 ng/mL or IFNβ (R&D Systems) at 200
569 IU/mL was performed in cDMEM plus 1% NEAA for 8 h. At respective time points, cells were
570 lysed for RNA extraction with Monarch Total RNA Miniprep Kit (New England Biolabs).
571
572 *Generation of HEV ΔORF2, ΔORF3, and GNN mutants*
573 Mutants were generated in the plasmid pBlueScript SK(+) encoding the HEV-3 Kernow-
574 C1/p6 sequence (pBSK-HEV-p6, GenBank accession number: JQ679013.1) by site-directed
575 mutagenesis. Mutations were introduced by overlap extension PCR with Phusion or Q5
576 polymerase (New England Biolabs) using the primers listed in Suppl. table 1, followed by
577 restriction enzyme digestion (New England Biolabs), ligation with T4 DNA Ligase (New England
578 Biolabs), transformation of JM109 competent cells (Promega), and validation by Sanger DNA
579 sequencing.

580 In vitro *transcription and EPO of HEV WT, ΔORF2, ΔORF3, and GNN mutants*
581 Plasmids were linearized with MluI and RNA was *in vitro* transcribed using the
582 mMESSAGE mMACHINE T7 kit (Invitrogen). $4x10^6$ HepG2/C3A cells were electroporated at
583 270 V and 975 µF with 10 µg of IVT HEV RNA in cytomix (120 mM KCl, 0.15 mM $CaCl_2$, 10 mM
584 KPO_4, 25 mM HEPES, 2 mM EGTA, and 5 mM $MgCl_2$), supplemented with adenosine
585 triphosphate (ATP) and glutathione (GT). After resuspension in cDMEM, HepG2/C3A cells
586 electroporated with HEV WT or mutants were mixed 1:1 with mock-electroporated cells. $2x10^5$
587 cells/well were seeded on 24-well plates for analysis by RT-qPCR and $1x10^5$ cells/well were
588 seeded on 48-well plates for analysis by RNA-FISH. One day post-EPO, all wells were washed
589 twice with PBS to remove inoculum and cDMEM was replaced. Cell lysates were harvested for
590 RNA extraction using the Universal RNA kit (Roboklon) according to manufacturer's instructions.
591 On day 1, day 3, and day 5 post-EPO, cDMEM was replaced and 6 µM TBK1 inhibitor BX795
592 (InvivoGen) or corresponding DMSO vehicle control was added to the wells dedicated to cell lysis
593 48 h later. Samples for RNA-FISH were fixed at respective time points with 4% paraformaldehyde
594 (PFA).
595
596 *EPO of Huh7.5 cells and IFN treatment*
597 Huh7.5 cells were electroporated with HEV WT or ΔORF2 IVT RNA as described above.
598 For time-course analysis, electroporated Huh7.5 cells were resuspended in cDMEM, seeded in
599 24-well plates, and harvested for RT-qPCR analysis at respective time points. For IFN treatment,
600 cells were plated in a T75 cell culture flask after EPO. On day 3 post-EPO, cells were reseeded
601 to 24-well plates at approximately 80% confluency. One day later, cells were treated with 10,000
602 IU/mL IFNα2A or 10 ng/mL IFNλ1. IFNs were replenished daily until cells were lysed for RNA
603 extraction with the Universal RNA kit (Roboklon) and RT-qPCR on day 7 post-EPO.
604
605 *ΔORF2 virus production by trans-complementation*
606 S10-3/ORF2 cells were electroporated with IVT ΔORF2 RNA and expanded on day 3 post-
607 EPO. Intracellular nHEV particles were harvested 7 days post-EPO from cell lysates by four
608 repeated freeze-thaw cycles and pelleted by ultracentrifugation at 28,000 rpm for 3 h through a
609 20% sucrose cushion. HEV WT and ΔORF2 genome copies were determined by RT-qPCR
610 following TRIzol extraction from the resuspended virus prep.
611
612 *Synchronized, time-resolved HEV infection*
613 $6x10^4$ HepG2/C3A cells were seeded on collagen-coated 24-well plates. The next day,
614 cells were infected with equal genome equivalents (GEs) of HEV WT or ΔORF2 virus (30 GE/cell).
615 Virus was bound at 4 °C for 2 h in Minimum Essential Medium (MEM, Gibco), supplemented with
616 10% FBS and 1% pen/strep, followed by internalization at 37 °C for 8 h. After internalization,
617 inoculum was removed, cells were washed twice with PBS, and cDMEM was added. Samples for
618 RT-qPCR were lysed at respective time points with TRIzol for RNA extraction.
619
620 *3'-targeted 10x Genomics and Illumina sequencing*
621 $8x10^4$ HepG2/C3A cells were seeded on collagen-coated 24-well plates, and synchronized
622 HEV infection was performed as described above. At 56 h and day 7 post-internalization, cells
623 were trypsinized for 10 min, gently resuspended, and singularized by pipetting thrice through a

70 µm cell strainer. Two wells of each sample were combined. Single-cell suspensions were washed once with 0.04% BSA in PBS and finally resuspended in 0.04% BSA in PBS. Cell suspension was counted and inspected for cell death using trypan blue. Single-cell suspensions were loaded onto the 10x Chromium controller according to manufacturer's instructions of the Chromium Next GEM Single Cell 3' Kit v3.1 (10x Genomics) with a targeted cell recovery of 5,000. Sequencing libraries were prepared according to the manufacturer's instructions. Briefly, GEMs were generated, reverse transcription was performed, GEMs were cleaned up, and cDNA was amplified and cleaned up with SPRIselect beads (Beckman Coulter). Quantification and quality control were performed using Qubit (Thermo Fisher Scientific) and the 5200 Fragment Analyzer System (Agilent Technologies). Fragmentation, end repair, and A-tailing were followed by SPRIselect-based cleanup, adaptor ligation, sample indexing, and again, SPRIselect cleanup. Quantification and quality control were performed with 5200 Fragment Analyzer System (Agilent Technologies) and NEBNext Library Quant Kit for Illumina (New England Biolabs). Resulting libraries were pooled and sequenced on Illumina NextSeq550 (high-output mode, paired-end, 150 cycles).

scRNA-seq data analysis

Fastq files were aligned and counted using the Cell Ranger 7.1.0 pipeline. As a human genome reference we used GRCh38-3.0.0. For the gene set enrichment analysis, up- and down-regulated genes were identified using a Wilcoxon rank sum test as implemented in the FindMarkers function from Seurat 5.0. We filtered out genes which were expressed in less than 5% of cells in either uninfected or infected samples and with p-adjusted values < 0.05. GSEA was performed using the enrichR v3.2 R package. As a reference we used the hallmark gene sets of the Human MSigDB Collections[38]. The entire analysis was carried out using R 4.3.3. For clustering and UMAP projections, we used only a subset of genes based on a list of ISGs reported by Schoggins *et al.*[39]. Counts were scaled and log1-normalized. The UMAP projections were calculated over the first 20 dimensions of the PCA, setting the following parameters: min.dist=0.5 and n.neighbors=200. In order to identify clusters associated with transcriptionally active/inactive states, we set a resolution of 0.1 in the FindClusters function and then we inspected the expression of ISGs in the identified clusters. For the DEA we used the FindMarkers function and filtered out genes expressed in less than 5% of cells in the compared conditions and with p-adjusted values < 0.05. For ISG expression we used AUC values to score cells based on the Schoggins signature mentioned above implemented with the AUCell 1.24.0 R package. For the comparison of the gene expression across conditions we used a two-sided Wilcoxon rank sum test. Binarized ORF2 expression was carried out by defining positive cells as those expressing at least one HEV RNA count. We used the Seurat 5.0 R package for the entire analysis. The data is accessible under the GEO accession number GSE288400.

Statistical analysis

Graphs were made and statistical analysis was performed using GraphPad Prism 8 or R 4.3.3 for the scRNA-seq analysis. Statistical tests and p-values are listed in the respective figure legends.

Acknowledgments

The authors gratefully acknowledge Dr. Suzanne Emerson, Dr. Rainer Ulrich, Dr. Frauke Mücksch, and Dr. Henrik Kaessmann for sharing reagents, and Andrew Freistaedter and Céline Schneider for excellent technical support. We acknowledge Dr. Vibor Laketa, head of the Infectious Diseases Imaging Platform (IDIP) at the University Hospital Heidelberg for expert support. The authors thank Dr. Marlène Dreux for critical reading of the manuscript. We thank the BIOI2 platform and the I2BC's IT support team for making AlphaFold 2.3 easily accessible at the I2BC.

Funding

A.M., S.S., C.R., C.H., M.B., and V.L.D.T were supported by grants from the Deutsche Forschungsgemeinschaft (DFG, German Research Foundation) – Projektnummer – 272983813 SFB/TRR 179. V.L.D.T. was additionally supported by the Chica and Heinz Schaller Foundation, DFG grant DA1640/3-1, and TTU Hepatitis Project 05.823. J.H. was supported by a fellowship from the China Scholarship Council.

Author contributions

Conceptualization, A.M., and V.L.D.T.; Methodology, A.M., S.S., C.R, V.G.M, C.S., A.L.C., J.H., and T.T.; Investigation, A.M., S.S, C.R., and T.T.; Resources: D.K., M.K., X.W.; Software, A.M., S.S., C.R., A.L.C., T.T.; Data analysis, A.M., S.S., C.R., A.L.C., C.H., J.H.; Writing original draft, A.M., and V.L.D.T.; Final draft, A.M., and V.L.D.T.; Supervision, C.H., B.M., V.L.D.T.; Funding, V.L.D.T.

Declaration of interests

All authors declare no conflict of interest

692 **References**

693 1 Horvatits, T., Schulze Zur Wiesch, J., Lütgehetmann, M., Lohse, A. W. & Pischke, S. The
694 Clinical Perspective on Hepatitis E. *Viruses* **11**, doi:10.3390/v11070617 (2019).
695 2 Nimgaonkar, I., Ding, Q., Schwartz, R. E. & Ploss, A. Hepatitis E virus: advances and
696 challenges. *Nat Rev Gastroenterol Hepatol* **15**, 96-110, doi:10.1038/nrgastro.2017.150
697 (2018).
698 3 Das, A., Rivera-Serrano, E. E., Yin, X., Walker, C. M., Feng, Z. & Lemon, S. M. Cell entry
699 and release of quasi-enveloped human hepatitis viruses. *Nature reviews. Microbiology* **21**,
700 573-589, doi:10.1038/s41579-023-00889-z (2023).
701 4 Hervouet, K., Ferrie, M., Ankavay, M., Montpellier, C., Camuzet, C., Alexandre, V.,
702 Dembele, A., Lecoeur, C., Foe, A. T., Bouquet, P., Hot, D., Vausselin, T., Saliou, J. M.,
703 Salome-Desnoulez, S., Vandeputte, A., Marsollier, L., Brodin, P., Dreux, M., Rouille, Y.,
704 Dubuisson, J., Aliouat-Denis, C. M. & Cocquerel, L. An Arginine-Rich Motif in the ORF2
705 capsid protein regulates the hepatitis E virus lifecycle and interactions with the host cell.
706 *PLoS Pathog* **18**, e1010798, doi:10.1371/journal.ppat.1010798 (2022).
707 5 Yin, X., Ying, D., Lhomme, S., Tang, Z., Walker, C. M., Xia, N., Zheng, Z. & Feng, Z.
708 Origin, antigenicity, and function of a secreted form of ORF2 in hepatitis E virus infection.
709 *Proc Natl Acad Sci U S A* **115**, 4773-4778, doi:10.1073/pnas.1721345115 (2018).
710 6 Montpellier, C., Wychowski, C., Sayed, I. M., Meunier, J. C., Saliou, J. M., Ankavay, M.,
711 Bull, A., Pillez, A., Abravanel, F., Helle, F., Brochot, E., Drobecq, H., Farhat, R., Aliouat-
712 Denis, C. M., Haddad, J. G., Izopet, J., Meuleman, P., Goffard, A., Dubuisson, J. &
713 Cocquerel, L. Hepatitis E Virus Lifecycle and Identification of 3 Forms of the ORF2 Capsid
714 Protein. *Gastroenterology* **154**, 211-223 e218, doi:10.1053/j.gastro.2017.09.020 (2018).
715 7 Ankavay, M., Montpellier, C., Sayed, I. M., Saliou, J. M., Wychowski, C., Saas, L., Duvet,
716 S., Aliouat-Denis, C. M., Farhat, R., de Masson d'Autume, V., Meuleman, P., Dubuisson,
717 J. & Cocquerel, L. New insights into the ORF2 capsid protein, a key player of the hepatitis
718 E virus lifecycle. *Sci Rep* **9**, 6243, doi:10.1038/s41598-019-42737-2 (2019).
719 8 Wu, J. & Chen, Z. J. Innate immune sensing and signaling of cytosolic nucleic acids. *Annu*
720 *Rev Immunol* **32**, 461-488, doi:10.1146/annurev-immunol-032713-120156 (2014).
721 9 Schneider, W. M., Chevillotte, M. D. & Rice, C. M. Interferon-stimulated genes: a complex
722 web of host defenses. *Annu Rev Immunol* **32**, 513-545, doi:10.1146/annurev-immunol-
723 032713-120231 (2014).
724 10 Yu, C., Boon, D., McDonald, S. L., Myers, T. G., Tomioka, K., Nguyen, H., Engle, R. E.,
725 Govindarajan, S., Emerson, S. U. & Purcell, R. H. Pathogenesis of hepatitis E virus and
726 hepatitis C virus in chimpanzees: similarities and differences. *J Virol* **84**, 11264-11278,
727 doi:10.1128/JVI.01205-10 (2010).
728 11 Yin, X., Li, X., Ambardekar, C., Hu, Z., Lhomme, S. & Feng, Z. Hepatitis E virus persists
729 in the presence of a type III interferon response. *PLoS Pathog* **13**, e1006417,
730 doi:10.1371/journal.ppat.1006417 (2017).
731 12 Wu, X., Dao Thi, V. L., Liu, P., Takacs, C. N., Xiang, K., Andrus, L., Gouttenoire, J.,
732 Moradpour, D. & Rice, C. M. Pan-Genotype Hepatitis E Virus Replication in Stem Cell-
733 Derived Hepatocellular Systems. *Gastroenterology* **154**, 663-674 e667,
734 doi:10.1053/j.gastro.2017.10.041 (2018).
735 13 Dao Thi, V. L., Debing, Y., Wu, X., Rice, C. M., Neyts, J., Moradpour, D. & Gouttenoire, J.
736 Sofosbuvir Inhibits Hepatitis E Virus Replication In Vitro and Results in an Additive Effect
737 When Combined With Ribavirin. *Gastroenterology* **150**, 82-85 e84,
738 doi:10.1053/j.gastro.2015.09.011 (2016).
739 14 Todt, D., Francois, C., Anggakusuma, Behrendt, P., Engelmann, M., Knegendorf, L.,
740 Vieyres, G., Wedemeyer, H., Hartmann, R., Pietschmann, T., Duverlie, G. & Steinmann,
741 E. Antiviral Activities of Different Interferon Types and Subtypes against Hepatitis E Virus

742 Replication. *Antimicrob Agents Chemother* **60**, 2132-2139, doi:10.1128/AAC.02427-15
743 (2016).
744 15 Debing, Y., Emerson, S. U., Wang, Y., Pan, Q., Balzarini, J., Dallmeier, K. & Neyts, J.
745 Ribavirin inhibits in vitro hepatitis E virus replication through depletion of cellular GTP
746 pools and is moderately synergistic with alpha interferon. *Antimicrob Agents Chemother*
747 **58**, 267-273, doi:10.1128/aac.01795-13 (2014).
748 16 Bruggemann, Y., Klohn, M., Wedemeyer, H. & Steinmann, E. Hepatitis E virus: from innate
749 sensing to adaptive immune responses. *Nat Rev Gastroenterol Hepatol*,
750 doi:10.1038/s41575-024-00950-z (2024).
751 17 Nan, Y., Yu, Y., Ma, Z., Khattar, S. K., Fredericksen, B. & Zhang, Y. J. Hepatitis E virus
752 inhibits type I interferon induction by ORF1 products. *J Virol* **88**, 11924-11932,
753 doi:10.1128/jvi.01935-14 (2014).
754 18 Kang, S., Choi, C., Choi, I., Han, K. N., Rho, S. W., Choi, J., Kwon, J., Park, M. K., Kim,
755 S. J. & Myoung, J. Hepatitis E Virus Methyltransferase Inhibits Type I Interferon Induction
756 by Targeting RIG-I. *J Microbiol Biotechnol* **28**, 1554-1562, doi:10.4014/jmb.1808.08058
757 (2018).
758 19 Kim, E. & Myoung, J. Hepatitis E Virus Papain-Like Cysteine Protease Inhibits Type I
759 Interferon Induction by Down-Regulating Melanoma Differentiation-Associated Gene 5. *J*
760 *Microbiol Biotechnol* **28**, 1908-1915, doi:10.4014/jmb.1809.09028 (2018).
761 20 Myoung, J. & Min, K. Dose-Dependent Inhibition of Melanoma Differentiation-Associated
762 Gene 5-Mediated Activation of Type I Interferon Responses by Methyltransferase of
763 Hepatitis E Virus. *J Microbiol Biotechnol* **29**, 1137-1143, doi:10.4014/jmb.1905.05040
764 (2019).
765 21 Bagdassarian, E., Doceul, V., Pellerin, M., Demange, A., Meyer, L., Jouvenet, N. & Pavio,
766 N. The Amino-Terminal Region of Hepatitis E Virus ORF1 Containing a Methyltransferase
767 (Met) and a Papain-Like Cysteine Protease (PCP) Domain Counteracts Type I Interferon
768 Response. *Viruses* **10**, doi:10.3390/v10120726 (2018).
769 22 Hingane, S., Joshi, N., Surjit, M. & Ranjith-Kumar, C. T. Hepatitis E Virus ORF2 Inhibits
770 RIG-I Mediated Interferon Response. *Front Microbiol* **11**, 656,
771 doi:10.3389/fmicb.2020.00656 (2020).
772 23 Lin, S., Yang, Y., Nan, Y., Ma, Z., Yang, L. & Zhang, Y. J. The Capsid Protein of Hepatitis
773 E Virus Inhibits Interferon Induction via Its N-terminal Arginine-Rich Motif. *Viruses* **11**,
774 doi:10.3390/v11111050 (2019).
775 24 Surjit, M., Varshney, B. & Lal, S. K. The ORF2 glycoprotein of hepatitis E virus inhibits
776 cellular NF-κB activity by blocking ubiquitination mediated proteasomal degradation of
777 IκBα in human hepatoma cells. *BMC biochemistry* **13**, 7, doi:10.1186/1471-2091-13-7
778 (2012).
779 25 Dong, C., Zafrullah, M., Mixson-Hayden, T., Dai, X., Liang, J., Meng, J. & Kamili, S.
780 Suppression of interferon-alpha signaling by hepatitis E virus. *Hepatology* **55**, 1324-1332,
781 doi:10.1002/hep.25530 (2012).
782 26 He, M., Wang, M., Huang, Y., Peng, W., Zheng, Z., Xia, N., Xu, J. & Tian, D. The ORF3
783 Protein of Genotype 1 Hepatitis E Virus Suppresses TLR3-induced NF-kappaB Signaling
784 via TRADD and RIP1. *Sci Rep* **6**, 27597, doi:10.1038/srep27597 (2016).
785 27 Lei, Q., Li, L., Zhang, S., Li, T., Zhang, X., Ding, X. & Qin, B. HEV ORF3 downregulates
786 TLR7 to inhibit the generation of type I interferon via impairment of multiple signaling
787 pathways. *Sci Rep* **8**, 8585, doi:10.1038/s41598-018-26975-4 (2018).
788 28 Nan, Y., Ma, Z., Wang, R., Yu, Y., Kannan, H., Fredericksen, B. & Zhang, Y. J.
789 Enhancement of interferon induction by ORF3 product of hepatitis E virus. *J Virol* **88**, 8696-
790 8705, doi:10.1128/jvi.01228-14 (2014).
791 29 Plociennikowska, A., Frankish, J., Moraes, T., Del Prete, D., Kahnt, F., Acuna, C., Slezak,
792 M., Binder, M. & Bartenschlager, R. TLR3 activation by Zika virus stimulates inflammatory

cytokine production which dampens the antiviral response induced by RIG-I-like receptors. *J Virol* **95**, doi:10.1128/JVI.01050-20 (2021).

30 Magalhães, V. G., Lukassen, S., Drechsler, M., Loske, J., Burkart, S. S., Wüst, S., Jacobsen, E. M., Röhmel, J., Mall, M. A., Debatin, K. M., Eils, R., Autenrieth, S., Janda, A., Lehmann, I. & Binder, M. Immune-epithelial cell cross-talk enhances antiviral responsiveness to SARS-CoV-2 in children. *EMBO reports* **24**, e57912, doi:10.15252/embr.202357912 (2023).

31 Joshi, G., Décembre, E., Brocard, J., Montpellier, C., Ferrié, M., Allatif, O., Mehnert, A.-K., Pons, J., Galiana, D., Dao Thi, V. L., Jouvenet, N., Cocquerel, L. & Dreux, M. Hepatitis E Virus-induced antiviral response by plasmacytoid dendritic cells is modulated by the ORF2 protein. 2024.2004.2012.589258, doi:10.1101/2024.04.12.589258 %J bioRxiv (2024).

32 Dao Thi, V. L., Wu, X., Belote, R. L., Andreo, U., Takacs, C. N., Fernandez, J. P., Vale-Silva, L. A., Prallet, S., Decker, C. C., Fu, R. M., Qu, B., Uryu, K., Molina, H., Saeed, M., Steinmann, E., Urban, S., Singaraja, R. R., Schneider, W. M., Simon, S. M. & Rice, C. M. Stem cell-derived polarized hepatocytes. *Nat Commun* **11**, 1677, doi:10.1038/s41467-020-15337-2 (2020).

33 Fu, R., Engels, Z., Weihs, J. A., Mürle, J., Klöhn, M., Todt, D., Hu, J., Steinmann, E., Böttler, T., Lozach, P.-Y., Lemon, S. M. & Thi, V. L. D. A high-content RNA-based imaging assay reveals integrin beta 1 as a cofactor for cell entry of non-enveloped hepatitis E virus. 2023.2010.2027.564362, doi:10.1101/2023.10.27.564362 %J bioRxiv (2023).

34 Sumpter, R., Jr., Loo, Y. M., Foy, E., Li, K., Yoneyama, M., Fujita, T., Lemon, S. M. & Gale, M., Jr. Regulating intracellular antiviral defense and permissiveness to hepatitis C virus RNA replication through a cellular RNA helicase, RIG-I. *J Virol* **79**, 2689-2699, doi:10.1128/JVI.79.5.2689-2699.2005 (2005).

35 Colasanti, O., Burm, R., Huang, H. E., Riedl, T., Traut, J., Gillich, N., Li, T. F., Corneillie, L., Faure-Dupuy, S., Grünvogel, O., Heide, D., Lee, J. Y., Tran, C. S., Merle, U., Chironna, M., Vondran, F. F. W., Esser-Nobis, K., Binder, M., Bartenschlager, R., Heikenwälder, M., Meuleman, P. & Lohmann, V. Comparison of HAV and HCV infections in vivo and in vitro reveals distinct patterns of innate immune evasion and activation. *J Hepatol* **79**, 645-656, doi:10.1016/j.jhep.2023.04.023 (2023).

36 Ding, Q., Heller, B., Capuccino, J. M., Song, B., Nimgaonkar, I., Hrebikova, G., Contreras, J. E. & Ploss, A. Hepatitis E virus ORF3 is a functional ion channel required for release of infectious particles. *Proc Natl Acad Sci U S A* **114**, 1147-1152, doi:10.1073/pnas.1614955114 (2017).

37 Moulin, C., Crupi, M. J. F., Ilkow, C. S., Bell, J. C. & Boulton, S. Extracellular Vesicles and Viruses: Two Intertwined Entities. *Int J Mol Sci* **24**, doi:10.3390/ijms24021036 (2023).

38 Liberzon, A., Birger, C., Thorvaldsdottir, H., Ghandi, M., Mesirov, J. P. & Tamayo, P. The Molecular Signatures Database (MSigDB) hallmark gene set collection. *Cell Syst* **1**, 417-425, doi:10.1016/j.cels.2015.12.004 (2015).

39 Schoggins, J. W. & Rice, C. M. Interferon-stimulated genes and their antiviral effector functions. *Curr Opin Virol* **1**, 519-525, doi:10.1016/j.coviro.2011.10.008 (2011).

40 Todt, D., Friesland, M., Moeller, N., Praditya, D., Kinast, V., Brüggemann, Y., Knegendorf, L., Burkard, T., Steinmann, J., Burm, R., Verhoye, L., Wahid, A., Meister, T. L., Engelmann, M., Pfankuche, V. M., Puff, C., Vondran, F. W. R., Baumgärtner, W., Meuleman, P., Behrendt, P. & Steinmann, E. Robust hepatitis E virus infection and transcriptional response in human hepatocytes. *Proc Natl Acad Sci U S A* **117**, 1731-1741, doi:10.1073/pnas.1912307117 (2020).

41 Sooryanarain, H., Heffron, C. L. & Meng, X. J. The U-Rich Untranslated Region of the Hepatitis E Virus Induces Differential Type I and Type III Interferon Responses in a Host Cell-Dependent Manner. *mBio* **11**, doi:10.1128/mBio.03103-19 (2020).

42 de Beijer, N. L., Snijder, E. J. & Bárcena, M. A Cool Look at Positive-Strand RNA Virus Replication Organelles: New Insights from Cryo-Electron Microscopy. *Annual review of biochemistry* **93**, 163-187, doi:10.1146/annurev-biochem-052521-115736 (2024).

43 Oechslin, N., Da Silva, N., Ankavay, M., Moradpour, D. & Gouttenoire, J. A genome-wide CRISPR/Cas9 screen identifies a role for Rab5A and early endosomes in hepatitis E virus replication. *Proc Natl Acad Sci U S A* **120**, e2307423120, doi:10.1073/pnas.2307423120 (2023).

44 Bentaleb, C., Hervouet, K., Montpellier, C., Camuzet, C., Ferrie, M., Burlaud-Gaillard, J., Bressanelli, S., Metzger, K., Werkmeister, E., Ankavay, M., Janampa, N. L., Marlet, J., Roux, J., Deffaud, C., Goffard, A., Rouille, Y., Dubuisson, J., Roingeard, P., Aliouat-Denis, C. M. & Cocquerel, L. The endocytic recycling compartment serves as a viral factory for hepatitis E virus. *Cell Mol Life Sci* **79**, 615, doi:10.1007/s00018-022-04646-y (2022).

45 Metzger, K., Bentaleb, C., Hervouet, K., Alexandre, V., Montpellier, C., Saliou, J. M., Ferrie, M., Camuzet, C., Rouille, Y., Lecoeur, C., Dubuisson, J., Cocquerel, L. & Aliouat-Denis, C. M. Processing and Subcellular Localization of the Hepatitis E Virus Replicase: Identification of Candidate Viral Factories. *Front Microbiol* **13**, 828636, doi:10.3389/fmicb.2022.828636 (2022).

46 Glitscher, M., Spannaus, I. M., Behr, F., Murra, R. O., Woytinek, K., Bender, D. & Hildt, E. The Protease Domain in HEV pORF1 Mediates the Replicase's Localization to Multivesicular Bodies and Its Exosomal Release. *Cell Mol Gastroenterol Hepatol* **17**, 589-605, doi:10.1016/j.jcmgh.2024.01.001 (2024).

47 Ankavay, M., Da Silva, N., Pollán, A., Oechslin, N., Dinkelborg, K., Behrendt, P., Moradpour, D. & Gouttenoire, J. Monitoring of Hepatitis E Virus Infection and Replication by Functional Tagging of the ORF2 Protein. *JHEP Reports*, doi:10.1016/j.jhepr.2024.101293.

48 Karpe, Y. A. Processing of the Hepatitis E virus ORF1 nonstructural polyprotein. *Frontiers in Virology* **3**, doi:10.3389/fviro.2023.1327745 (2024).

49 Meylan, E., Curran, J., Hofmann, K., Moradpour, D., Binder, M., Bartenschlager, R. & Tschopp, J. Cardif is an adaptor protein in the RIG-I antiviral pathway and is targeted by hepatitis C virus. *Nature* **437**, 1167-1172, doi:10.1038/nature04193 (2005).

50 Yang, Y., Liang, Y., Qu, L., Chen, Z., Yi, M., Li, K. & Lemon, S. M. Disruption of innate immunity due to mitochondrial targeting of a picornaviral protease precursor. *Proc Natl Acad Sci U S A* **104**, 7253-7258, doi:10.1073/pnas.0611506104 (2007).

51 Shafat, Z., Ahmed, A., Parvez, M. K. & Parveen, S. Intrinsic disorder in the open reading frame 2 of hepatitis E virus: a protein with multiple functions beyond viral capsid. *Journal, genetic engineering & biotechnology* **21**, 33, doi:10.1186/s43141-023-00477-x (2023).

52 Ferrie, M., Alexandre, V., Montpellier, C., Bouquet, P., Tubiana, T., Meziere, L., Ankavay, M., Bentaleb, C., Dubuisson, J., Bressanelli, S., Aliouat-Denis, C. M., Rouille, Y. & Cocquerel, L. The AP-1 adaptor complex is essential for intracellular trafficking of the ORF2 capsid protein and assembly of Hepatitis E virus. *Cell Mol Life Sci* **81**, 335, doi:10.1007/s00018-024-05367-0 (2024).

53 Bret, H., Gao, J., Zea, D. J., Andreani, J. & Guerois, R. From interaction networks to interfaces, scanning intrinsically disordered regions using AlphaFold2. *Nat Commun* **15**, 597, doi:10.1038/s41467-023-44288-7 (2024).

54 Versini, R., Sritharan, S., Aykac Fas, B., Tubiana, T., Aimeur, S. Z., Henri, J., Erard, M., Nüsse, O., Andreani, J., Baaden, M., Fuchs, P., Galochkina, T., Chatzigoulas, A., Cournia, Z., Santuz, H., Sacquin-Mora, S. & Taly, A. A Perspective on the Prospective Use of AI in Protein Structure Prediction. *Journal of chemical information and modeling* **64**, 26-41, doi:10.1021/acs.jcim.3c01361 (2024).

55 Arai, M., Suetaka, S. & Ooka, K. Dynamics and interactions of intrinsically disordered proteins. *Current opinion in structural biology* **84**, 102734, doi:10.1016/j.sbi.2023.102734 (2024).

56 Hato, S. V., Ricour, C., Schulte, B. M., Lanke, K. H., de Bruijni, M., Zoll, J., Melchers, W. J., Michiels, T. & van Kuppeveld, F. J. The mengovirus leader protein blocks interferon-alpha/beta gene transcription and inhibits activation of interferon regulatory factor 3. *Cell Microbiol* **9**, 2921-2930, doi:10.1111/j.1462-5822.2007.01006.x (2007).

Figures

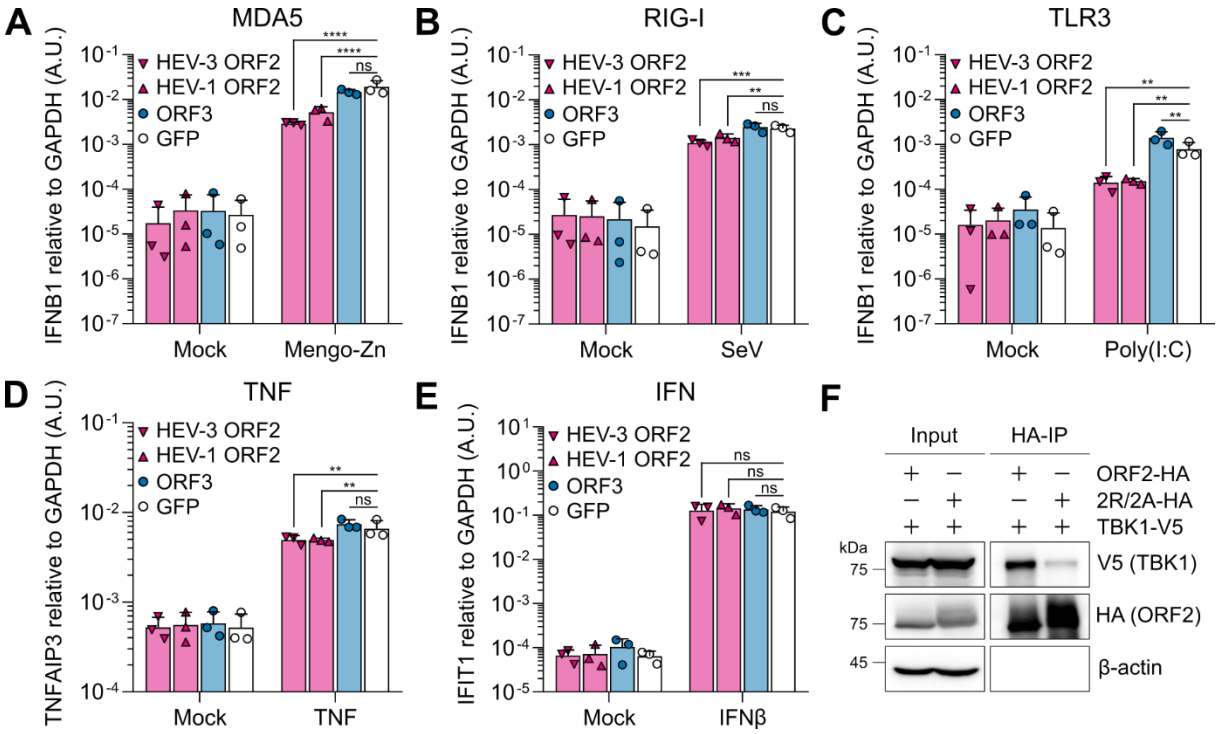

Figure 1: The HEV ORF2 protein antagonizes both antiviral and inflammatory signaling pathways and interacts with TBK1.

(A) A549 cells harboring knockouts of the PRRs RIG-I and MDA5 and ectopically expressing a single PRR (MDA5, RIG-I, or TLR3) together with either HEV-3 ORF2, HEV-1 ORF2, ORF3, or GFP were challenged with either Mengo-Zn virus at MOI 1 for 24 h, (B) Sendai virus (SeV) at MOI 0.75 for 4 h, or (C) 50 µg/mL poly(I:C) supernatant feeding for 24 h, as indicated. (D) A549-derived cells ectopically expressing MDA5 were stimulated with 10 ng/mL TNF or (E) 200 IU/mL IFNβ for 8 h. At respective time points, (A-C) *IFNB1*, (D) *TNFAIP3*, and (E) *IFIT1* expression were analyzed by RT-qPCR, each relative to the housekeeping gene *GAPDH* using the $2^{-\Delta Ct}$ method. Data show mean ± SD of n = 3 independent biological experiments. Statistical analysis was performed using two-way ANOVA. **: $p < 0.01$; ***: $p < 0.001$; ****: $p < 0.0001$; ns, non-significant. A.U., arbitrary units. (F) HEK293T cells were co-transfected with ORF2-HA or ORF2-2R/2A-HA and TBK1-V5 and lysed 24 h post-transfection. Anti-HA co-IP and WB analysis for TBK1 (anti-V5 staining), ORF2 (anti-HA staining), and β-actin were performed. Shown is a representative blot of n = 3 independent biological experiments.

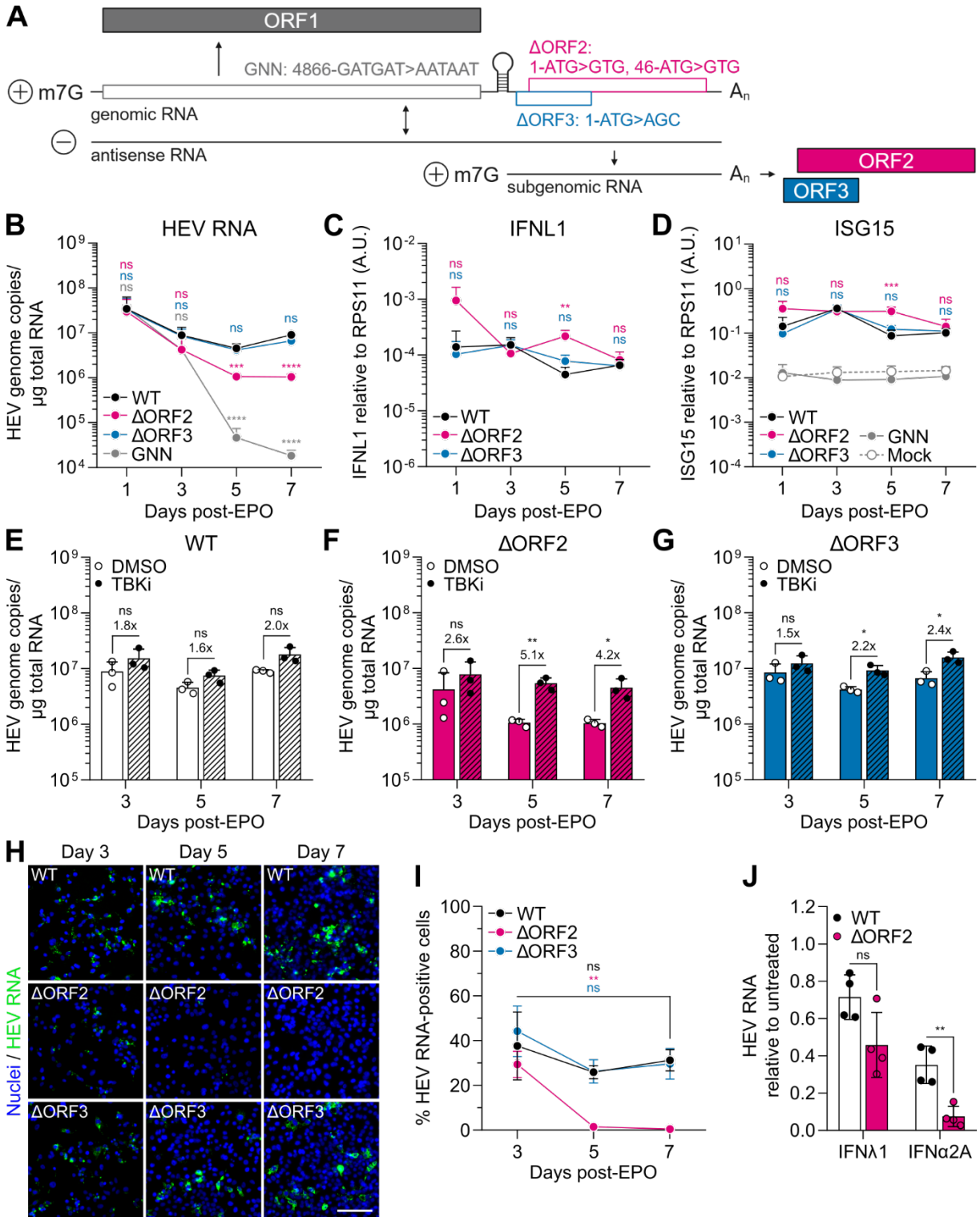

Figure 2: The capsid protein ORF2, but not the ORF3 protein, is pivotal for efficient HEV replication in immunocompetent cells.

(A) Schematic representation of the HEV genome and its replication intermediates. Nucleic acid positions of GNN mutation and start codon mutations of ΔORF2 and ΔORF3 mutants are indicated. m7G, 7-methylguanosin cap; A_n, poly(A)-tail. Created in BioRender. Dao Thi, V. (2025) https://BioRender.com/j85i934 (B) HepG2/C3A cells were electroporated with *in vitro* transcribed (IVT) HEV

927 WT, ΔORF2, ΔORF3, or replication-incompetent GNN RNA and analyzed by RT-qPCR at indicated time
928 points post-EPO for HEV RNA, (C) *IFNL1* expression over the housekeeping gene *RPS11* using the $2^{-\Delta Ct}$
929 method, and (D) *ISG15* expression over the housekeeping gene *RPS11* using the $2^{-\Delta Ct}$ method. *IFNL1*
930 expression was undetectable in mock and GNN samples. Data show mean ± SD of n = 3 independent
931 biological experiments. Statistical analysis over WT was performed using one-way ANOVA of each time
932 point independently and is indicated above the respective time points in the corresponding color. **: $p <$
933 0.01; ***: $p < 0.001$; ****: $p < 0.0001$; ns, non-significant. A.U., arbitrary units. (E-G) Electroporated
934 HepG2/C3A cells from (B) were additionally treated with 6 μM of the TBK1 inhibitor BX795 (TBKi) or
935 respective DMSO vehicle control 48 h prior to the indicated time point post-EPO. HEV RNA was quantified
936 by RT-qPCR and fold changes over DMSO treatment are shown above the respective graphs. Data show
937 mean ± SD of n = 3 independent biological experiments. Statistical analysis was performed using unpaired
938 two-tailed Student's t-test of each time point independently. *: $p < 0.05$; **: $p < 0.01$; ns, non-significant. (H)
939 Electroporated HepG2/C3A cells from (B) were stained for HEV RNA using RNA-FISH at indicated days
940 post-EPO. Images show exemplary images of n = 3 independent biological experiments. Scale bar, 100
941 μm. (I) The percentages of electroporated HepG2/C3A cells positive for HEV RNA, stained by RNA-FISH
942 in (H), were quantified with ilastik and CellProfiler. Data show mean ± SEM of n = 3 independent biological
943 experiments and 5 images quantified per experiment. Statistical analysis was performed using unpaired
944 two-tailed Student's t-test of each condition independently and is indicated in the corresponding color. **: p
945 < 0.01; ns, non-significant. (J) Huh7.5 cells were electroporated with IVT HEV WT or ΔORF2 RNA and
946 treated with 10 ng/mL IFNλ1 or 10,000 IU/mL IFNα2A from day 4 to day 7 post-EPO. IFNs were replenished
947 every 24 h. HEV RNA was quantified by RT-qPCR on day 7 post-EPO and normalized over the respective
948 untreated condition. Data show mean ± SD of n = 4 biological repeats from two independent biological
949 experiments. Statistical analysis was performed using unpaired two-tailed Student's t-test of IFNλ1 and
950 IFNα2A independently. **: $p < 0.01$; ns, non-significant.
951
952

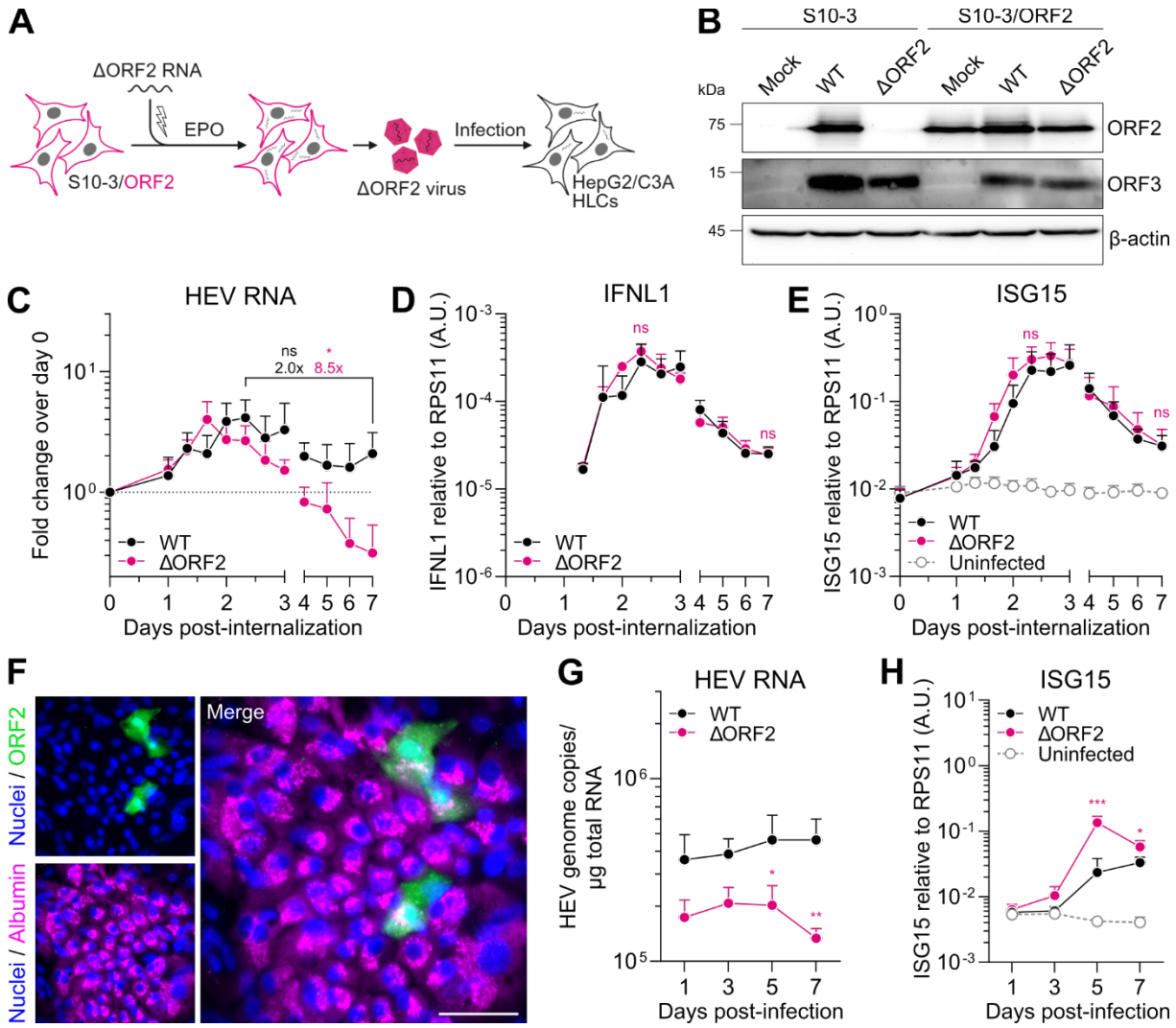

Figure 3: A balance between HEV replication and the antiviral response at an early infection bottleneck is essential for sustained viral replication.
(A) Schematic of ΔORF2 trans-complementation. S10-3 cells stably expressing HEV ORF2 were electroporated with ΔORF2 HEV RNA to produce virus particles containing the ΔORF2 genome packaged in capsid ORF2 protein expressed by the producer cell. Trans-complemented ΔORF2 virus was then used to infect HepG2/C3A cells or stem cell-derived HLCs. Created in BioRender. Dao Thi, V. (2025) https://BioRender.com/u54x394 (B) WB analysis of mock, WT-, or ΔORF2-electroporated S10-3 or S10-3/ORF2 cells for ORF2, ORF3, and β-actin protein expression. (C) Equal genome copies of HEV WT and ΔORF2 virus particles (30 GE/cell) were bound on HepG2/C3A cells for 2 h at 4 °C prior to internalization at 37 °C for 8 h, followed by removal of inoculum (= day 0). RT-qPCR was performed at indicated time points post-internalization to determine fold viral replication over day 0, (D) *IFNL1* expression over the housekeeping gene *RPS11* using the $2^{-\Delta Ct}$ method, and (E) *ISG15* expression over the housekeeping gene *RPS11* using the $2^{-\Delta Ct}$ method. *IFNL1* expression was undetectable in the uninfected sample. Statistical analysis of fold changes over time (C) and ΔORF2 compared to WT (D-E) are indicated above the respective time points in the corresponding color. Data show mean ± SD of n = 3 independent biological experiments. Statistical analysis was performed using unpaired two-tailed Student's t-test of the respective conditions or days independently. *: $p < 0.05$; ns, non-significant. A.U., arbitrary units; n/d, not detectable. (F) Exemplary image of stem cell-derived hepatocyte-like cells (HLCs) infected with HEV WT, fixed, and stained for albumin and ORF2 by immunofluorescence. Scale bar, 50 µm. (G) Stem cell-derived HLCs were infected with equal genome copies of HEV WT and ΔORF2 virus particles (30 GE/cell) and analyzed by

975 RT-qPCR for HEV RNA and (H) *ISG15* expression over the housekeeping gene *RPS11* using the $2^{-\Delta Ct}$
976 method. Data show mean ± SD of n = 4 biological replicates of two independent HLC differentiations.
977 Statistical analysis of ΔORF2 compared to WT was performed using unpaired two-tailed Student's t-test of
978 each time point independently. *: $p < 0.05$; **: $p < 0.01$; ***: $p < 0.001$.

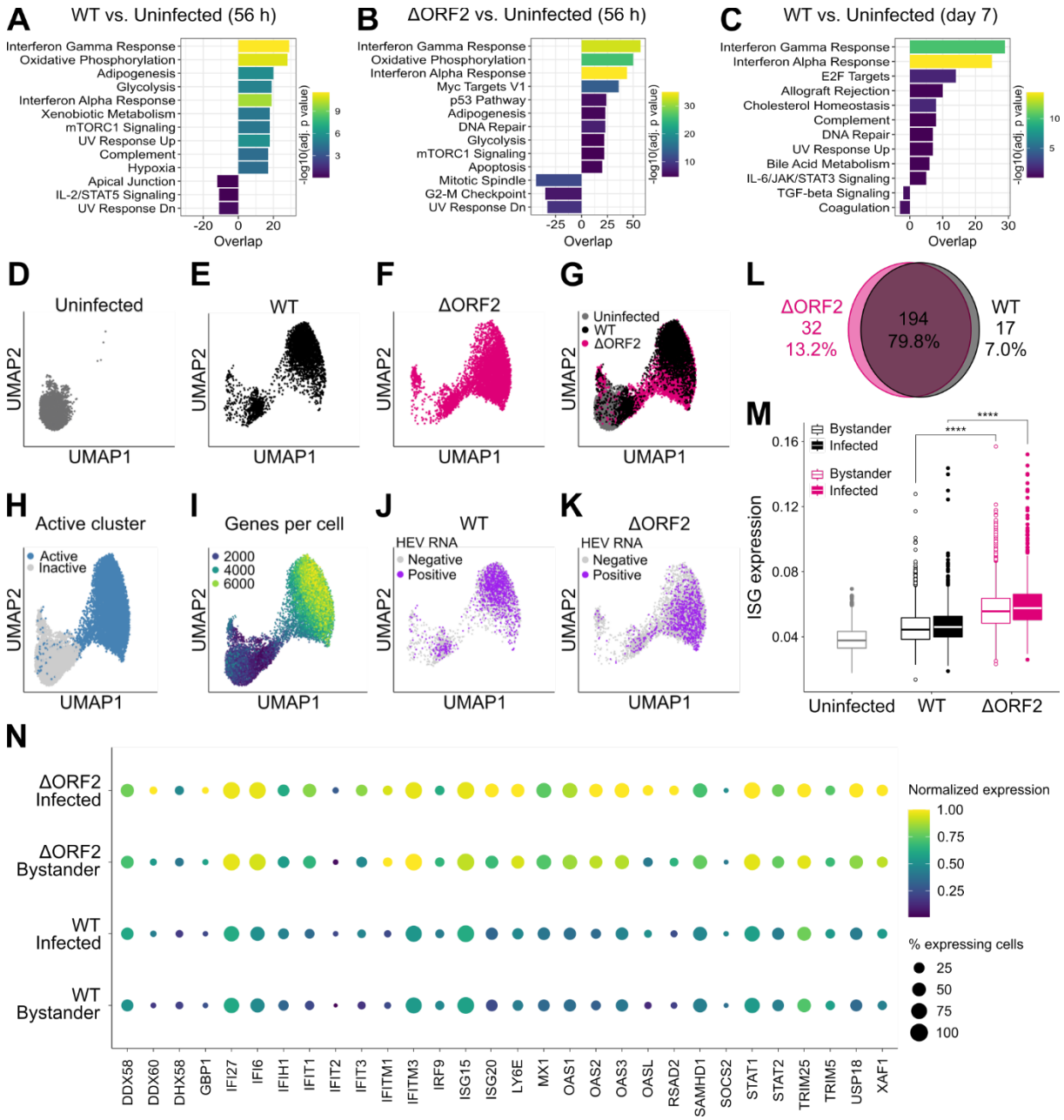

Figure 4: scRNA-seq analysis reveals globally dampened and partly divergent ISG responses in HEV-infected cells and bystanders in the presence of ORF2.

(A) Uninfected, WT-infected and ΔORF2-infected HepG2/C3A cells were harvested and processed by microfluidics-based 3'-targeted 10x Genomics at 56 h post-synchronized infection. Uninfected and WT-infected HepG2/C3A cells were also analyzed on day 7 post-synchronized infection. Gene set enrichment analysis comparing WT-infected with uninfected sample at 56 h post-infection, (B) ΔORF2-infected with uninfected sample at 56 h, and (C) WT-infected with uninfected sample on day 7 post-infection based on the hallmark gene sets of the hallmark gene sets of the Human MSigDB Collections[38] was performed. (D) UMAP projections of uninfected, (E) WT-infected, or (F) ΔORF2-infected HepG2/C3A cells harvested at 56 h post-synchronized infection. UMAPs were generated by clustering of all cells based on a list of approximately 400 ISGs published previously by Schoggins *et al.*[39] (G) Combined UMAP projections of

992 uninfected, WT-, and ΔORF2-infected samples, colored by condition. (H) Cells with upregulated ISG
993 expression are highlighted in UMAP projections of uninfected, WT-, and ΔORF2-infected samples in blue,
994 representing the active cluster. (I) UMAP projection of uninfected, WT-, and ΔORF2-infected samples,
995 highlighting the number of genes detected per cell in all samples. (J) UMAP projections of the WT-infected
996 and (K) ΔORF2-infected samples with indicated binarized HEV RNA counts in purple. (L) Differentially
997 expressed ISGs in the active clusters of WT- and ΔORF2-infected samples were compared and plotted in
998 a Venn diagram. Absolute numbers and percentages of shared and distinct differentially expressed ISGs
999 are shown. (M) Global changes in the ISG response were analyzed by comparison of normalized ISG
1000 expression across all samples (Uninfected, WT, and ΔORF2), based on a list of approximately 400 ISGs.
1001 WT- and ΔORF2-infected samples were split into actively infected cells, defined by detection of at least one
1002 HEV RNA copy per cell, and uninfected bystanders. Statistical analysis was performed using a two-sided
1003 Wilcoxon rank sum test. ****: $p < 0.0001$. (N) Out of the overlapping, differentially expressed ISGs between
1004 the active clusters of WT- and ΔORF2-infected samples, 30 ISGs were selected. Normalized expression
1005 and the percentage of cells were plotted for WT- and ΔORF2-infected samples, split by actively infected
1006 cells (at least one HEV RNA count per cell) and uninfected bystanders.

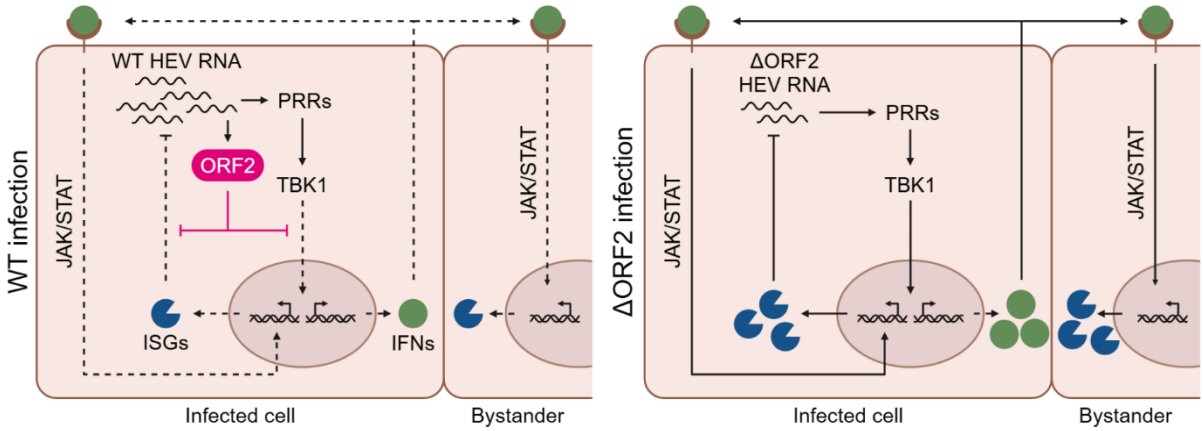

Figure 5: Working model of HEV ORF2 enabling persistent viral replication by dampening the cell-intrinsic antiviral response.

ORF2 directly interferes with IFN induction downstream of PRR recognition of HEV RNA in WT-infected cells, at least in part through direct interaction with TBK1. Consequently, ISG induction downstream of PRR signaling as well as IFN secretion and thus, autocrine and paracrine ISG induction downstream of the IFN receptor is dampened in infected cells and bystanders, respectively. Additionally, ORF2 shields HEV RNA from the antiviral functions of ISGs. In ΔORF2-infected cells, the lack of ORF2 results in stronger ISG induction downstream of PRR signaling as well as enhanced IFN secretion, leading to a stronger autocrine and paracrine ISG induction downstream of IFN signaling. Viral replication is consequently dampened as a result of the actions of antiviral effectors. Created in BioRender. Dao Thi, V. (2025) https://BioRender.com/h01q004